BMC Plant Biology

RESEARCH

Open Access

A three-way transcriptomic crosstalk interaction in a biocontrol agent (*Bacillus velezensis*), a fungal pathogen (*Colletotrichum gloeosporioides*), and a walnut host (*Juglans regia* L.)

Shiwei Wang[1], Hanmingyue Zhu[1], Shuying Li[1,2] and Tianhui Zhu[1,2*]

Abstract

Walnut anthracnose, caused by *Colletotrichum gloeosporioides*, is a globally significant disease. *Bacillus velezensis* demonstrates strong inhibitory effects against *C. gloeosporioides*. Current research primarily focuses on interactions between two species, leaving the molecular mechanisms of three-way interactions among walnut, pathogen, and biocontrol agent unexplored. To elucidate the molecular mechanisms in the "Walnut-*C. gloeosporioides*-*B. velezensis*" system, we employed three-way RNA-Seq to obtain transcriptome data for each species. We identified 111,674, 799, and 79 differentially expressed genes (DEGs) in walnut, *C. gloeosporioides*, and *B. velezensis* respectively. By integrating WGCNA and PPI network analyses, we discovered 3 key modules and 10 hub genes in *C. gloeosporioides*, and 2 key modules and 2 hub genes in *B. velezensis*. Functional enrichment analyses (GO and KEGG) revealed that walnut DEGs were enriched in secondary metabolism, disease-resistance proteins, plant hormone signal transduction, and pathogenesis-related proteins; *C. gloeosporioides* DEGs were associated with binding, antigen processing and presentation, and regulation of actin cytoskeleton; *B. velezensis* DEGs were linked to transmembrane transport, amino acid biosynthesis, carbon metabolism, and TCA cycle. These results demonstrate that the transcriptional responses of the three species mutually influence each other within the three-way system. This study addresses knowledge gaps in the biocontrol-pathogen-host interaction and provides a theoretical foundation for developing environmentally sustainable strategies to control walnut anthracnose.

Keywords *Colletotrichum gloeosporioides*, *Bacillus velezensis*, Three-way transcriptomic analysis, Plant-microbe interactions, *Juglans regia* L.

*Correspondence:
Tianhui Zhu
zhuth1227@126.com
[1]College of Forestry, Sichuan Agricultural University, Chengdu, Sichuan Province 611130, China
[2]National Forestry and Grassland Administration Key Laboratory of Forest Resources Conservation and Ecological Safety on the Upper Reaches of the Yangtze River, Chengdu, Sichuan Province, China

Background

Colletotrichum gloeosporioides ranks among the most destructive and globally prevalent plant pathogens. It infects a wide range of herbaceous and woody plants, including grapes, strawberries, mangoes, citrus fruits, and walnuts [1–5]. As a typical hemi-biotrophic pathogen, it penetrates plant epidermal cells through appressoria, forms infection vesicles and primary hyphae, and damage host tissues. Subsequently, secondary hyphae emerge as they enter the necrotrophic stage, obtaining nutrients from dead host cells [6].

Walnut (*Juglans regia* L.), one of the four globally significant nuts, is associated with potential health benefits such as retarding brain aging and cancer prevention [7]. However, walnut anthracnose caused by *C. gloeosporioides* severely damage leaves, fruits, and branches, significantly impeding growth and yield [5]. Plants deploy defense mechanisms against pathogens, including pathogen/microbe-associated molecular patterns (PAMPs/MAMPs), pattern-triggered immunity (PTI/MTI), effector-triggered immunity (ETI), systemic acquired resistance (SAR), and induced systemic resistance (ISR) mediated by beneficial bacteria [8]. Biocontrol agents such as *Bacillus* spp. enhance plant growth and induce systemic resistance, improving resilience against pathogens [9, 10]. Notably, *Bacillus velezensis* exhibits potent antibacterial activity against *C. gloeosporioides* through secondary metabolites like lipopeptides, chitinases, proteases, and β-1,3-glucanases [9, 11, 12].

RNA-Seq technology has been widely applied to study host-pathogen interactions. While conventional RNA-Seq focuses on single-species transcriptomes, three-way transcriptomic analysis enables simultaneous profiling of host plants and multiple microorganisms, thus deciphering dynamic gene regulatory interactions across these biological entities. For instance, *Bacillus* spp. were found to inhibit mycelial infection in the control of wheat take-all disease by regulating pathogen-derived abscisic acid [13]. Similarly, in grapes, the biocontrol agent *Pythium oligandrum* indirectly influenced the transcriptome of the fungal pathogen *Phaeomoniella chlamydospora*, regulating virulence genes and activating the JA/ET signaling pathway [14]. However, the molecular mechanisms underlying the tripartite interactions among walnuts, *C. gloeosporioides*, and *B. velezensis* remain unexplored. Investigating dynamic gene regulatory networks across tripartite species systems can provide a pathway for identifying cross-species target genes, thereby informing the development of ecologically sustainable long-term control strategies through multi-species co-regulatory mechanisms.

In this study, we investigated the "Walnut-*Colletotrichum gloeosporioides-Bacillus velezensis*" system using absolute quantification-based three-way transcriptome sequencing. Leaf samples were categorized into four groups: control (CK, no inoculation, denoted as C), *C. gloeosporioides*-inoculation (Cgp, T), *B. velezensis*-inoculation (Bv, B), and co-inoculation (Cgp & Bv, TB). Through this three-way interaction analysis, our objectives were to: (1) elucidate the effects of *C. gloeosporioides* and *B. velezensis* on walnut defense genes, (2) determine the inhibitory impact of *B. velezensis* on *C. gloeosporioides* pathogenesis, and (3) analyze the fungal counteractive effects on *B. velezensis* biocontrol activity. This integrated approach provides novel insights into the transcriptomic regulation of walnut anthracnose and to propose novel strategies for its biological control.

Methods

Plant materials and microbial strains

C. gloeosporioides and *B. velezensis* were provided by the Forest Protection Laboratory of the Forestry College at Sichuan Agricultural University. The experimental plants were 5-year-old "Xiangling" walnut trees (*Juglans regia* L.) cultivated in an experimental greenhouse.

Bacterial and fungal preparation

B. velezensis was cultured overnight at 30 °C in LB with shaking (200 rpm). The cells were harvested by centrifugation (8,000×g, 10 min), washed twice with sterile distilled water, and resuspended in sterile water to a final concentration of 1.0×10^8 CFU/mL. *C. gloeosporioides* was grown on potato dextrose agar (PDA) at 28 °C for 7 ~ 10 days until sporulation. The medium surface was repeatedly rinsed with sterile water to collect the spores, and the spore suspension was adjusted to a concentration of 1.0×10^6 spores/mL using a hemocytometer.

Interaction transcriptome sequencing was performed on four treatment groups: (1) untreated controls (CK, C); (2) *C. gloeosporioides* inoculation only (Cgp, T); (3) *B. velezensis* inoculation only (Bv, B); (4) co-inoculation with both strains (Cgp & Bv, TB) (Fig. S1). Each treatment group contained 15 uniformly sized walnut trees (mean height = 1.1 m). To prevent cross-contamination, groups were physically separated using transparent plastic barriers. Dual inoculation was performed every 3 days through foliar spray (500 mL/plant) and root drenching (500 mL/plant), totaling three applications. Following the final treatment, plants were maintained until day 12 post-inoculation. For RNA sequencing, six biological replicates were collected per treatment. From each of six randomly selected trees per group, six leaves of uniform size are collected from the same position. Leaves were pooled into composite sample, from which 15 leaves were randomly selected and divided into three 5-leaf aliquots ($n = 3$ technical replicates per treatment). All samples were immediately frozen in liquid nitrogen using

pre-chilled RNase-free cryovials and stored at -80 °C until RNA extraction.

Total RNA extraction, library construction, and sequencing

Total RNA was extracted using the Trizol extraction method following the manufacturer's protocol. RNA integrity was verified by 1.2% agarose gel electrophoresis, and concentration was quantified using NanoDrop 2000 (Thermo Fisher Scientific). After passing quality control (RIN ≥ 7.0), stranded RNA libraries were prepared using KC-Digital™ Total RNA Library Prep Kit (Catalog NO. DLR08702, Wuhan Seqhealth Co., Ltd., China), the MICROBExpress Kit (Thermo#AM1905), and the Ribo-off rRNA Depletion Kit (Bacteria) (Vazyme#N407). Unique Molecular Identifiers (UMIs) containing 8 random bases to label the pre-amplified cDNA molecules were incorporated during pre-amplification to mitigate PCR duplication artifacts. RNA Integrity was confirmed by 5300 Fragment Analyzer system (Agilent). Qualified RNAs were finally quantified by Qubit3.0 with QubitTM RNA Broad Range Assay kit (Life Technologies, Q10210). The library products corresponding to 200–500 bps were enriched, quantified and finally sequenced on Novaseq 6000 sequencer (Illumina) with PE150 model. The sequences are available in the National Center for Biotechnology Information (NCBI) databases under the accession number PRJNA1030780 and PRJNA1216589.

Three-way transcriptomic data analysis

Upon acquisition of the raw sequencing data (raw data), the initial step is to conduct quality control filtering of the raw data. The fastp software (version 0.23.0) is employed to eliminate low-quality reads. Clean reads are subsequently clustered based on their UMI sequences, with reads sharing identical UMI sequences being assigned to the same cluster. Within each cluster, reads are compared via pairwise alignment. Subsequently, reads exhibiting a sequence identity exceeding 95% are extracted and grouped into a new sub-cluster. Once all sub-groups are generated, multiple sequence alignment is executed to derive a consensus sequence for each sub-group. The reference genomes of the three species were merged. Subsequently, the STAR software (version 2.5.3a) was utilized to map the duplicate data onto the reference genomes of *C. gloeosporioides* (GCF_011800055.1), *Bacillus velezensis* (GCF_002117165.1), and *Juglans regia* L. (GCF_001411555.2). Transcriptome expression, annotation, and differential analysis were respectively performed for each species.

Gene expression, differential gene expression analysis

The reads mapped to the exon regions of each gene were counted using featureCounts (Subread v1.5.1; Bioconductor), and the RPKM (reads per kilobase per million mapped reads), calculated as (total exon reads / total mapped reads in millions) × (exon length in kilobases) [15]. Differentially expressed genes (DEGs) across groups were identified using the 'edgeR' package (v3.28.1). DEGs were filtered with thresholds of $|\log_2(\text{fold change})| > 1$ (equivalent to 2-fold change) and a false discovery rate (FDR)-adjusted $P < 0.05$. Hierarchical clustering was performed on $\log_{10}$-transformed RPKM values to classify distinct gene expression patterns. A heatmap of the clustered DEGs was generated to visualize global expression profiles.

Functional pathways and network interaction analyses of differentially expressed genes (DEGs)

Gene Ontology (GO) and Kyoto Encyclopedia of Genes and Genomes (KEGG) pathway enrichment analyses of differentially expressed genes (DEGs) were conducted using the KOBAS software (v2.1.1), with a significance threshold of $P \leq 0.05$.

Protein-protein interaction (PPI) networks of DEGs were constructed using the STRING database (v11.5; http://string-db.org/) with a confidence score threshold ≥ 0.4. For species with pre-existing PPI data in STRING, interactions associated with DEGs were retrieved to build the network. The PPI network was visualized and further analyzed using Cytoscape (v3.10.3; http://www.cytoscape.org/). Topological properties of the PPI network, including node degree, betweenness centrality, closeness centrality, and clustering coefficient, were calculated to identify hub genes (key nodes) within the network.

Construction and analysis of co-expression networks

Weighted gene co-expression network analysis (WGCNA) was mainly performed using the WGCNA package in R (v4.3.1) [16], with computational support from the Kangce Cloud Analysis Platform (KCCloud; http://www.seqcloud.cc:8888). The power value with a scale-free topology fitting index R^2 greater than 0.8 was selected as the soft threshold β to construct a scale-free network. The minimum height for merging modules was set to 0.25, and the weight threshold parameter was set to 0.8. Module-trait associations were evaluated by Pearson correlations between module eigengenes and experimental treatments. Significant modules with $r > 0.5$ and FDR-adjusted $P < 0.05$ were selected for further analysis. Intramodular connectivity of genes was quantified using the CytoHubba plugin in Cytoscape (v.3.10.3) [17].

Verification of transcriptome sequencing results using quantitative real-time polymerase chain reaction (qRT-PCR)

To evaluate the reliability of the transcriptome sequencing results, ten differentially expressed genes were selected from each species. For *Juglans regia* L., *C.*

gloeosporioides, and *B. velezensis*, GAPDH, *β*-tubulin, and 16S rRNA were used as internal reference genes for qRT-PCR verification, respectively. Gene-specific primers were designed using Primer Premier 5 and Oligo 7 (Table 1). SYBR Green I dye-based detection was performed using Hieff UNICON® Universal Blue qPCR SYBR Green Master Mix (Yeasen Biotechnology, Shanghai, China). Gene expression levels were analyzed on a Bio-Rad CFX96 Real-Time System with the following: 95 °C for 2 min (initial denaturation), 40 cycles of 95 °C for 10 s (denaturation) and 60 °C for 30 s (annealing/extension), followed by melting curve analysis. The relative expression levels were calculated using the $2^{-\Delta\Delta Ct}$ method.

Results

Three-way transcriptome sequencing of the "Walnut-*C. gloeosporioides*-*B. velezensis*" system

In subsequent experiments, walnut samples were divided into four groups: non-inoculated controls (CK, C), *C. gloeosporioides*-inoculated (Cgp, T), *B. velezensis*- inoculated (Bv, B), co-inoculated (Cgp & Bv, TB). After quality filtering of sequencing data from twelve biological replicates, the clean read counts averaged 64,878,286.00 (C), 49,438,552.67 (T), 60,978,869.33 (B), and 67,248,524.00 (TB). Sequencing quality metrics showed Q20 scores > 97%, Q30 scores > 92%, and GC content ranging from 45.51 to 46.55%. Reference genome alignment rates were > 92% for *Juglans regia* L., > 89% for *C. gloeosporioides*, and > 63% for *B. velezensis* (Table S1), confirming data reliability for downstream bioinformatics analysis.

Table 1 Primers sequences for the differentially expressed genes

Object	Gene	Upstream primer (5′-3′)	Downstream primer (5′-3′)
Juglans regia L.	GAPDH	TTAGATAATGTTCGACCTG	CTGTAGACCGAAATTGCTA
	LOC109001182	AAGGGTACTCAGTGGCTTCAG	TGAACACGTCCCCATTGTTG
	LOC108991632	TGGTGTCTCAAAAGCCAAGC	TGCCCAAGATCAAGGTGTTC
	LOC108998651	ATGCATCACTTGGTCGGTTG	TGGCCCATGTGATTTTTCGC
	LOC109011187	ACGTGTCACCTCCCTATTTGTC	CGACGCCGTTAAAGAGCTTAAC
	LOC109013811	CTCGTAACCAATCACAGTTGCC	ACCCACGACAACAACACAAC
	LOC108982886	ACTGCTGTAGACGTGAATCGAG	AGAAGCCTCAGCCTTTCCAC
	LOC109021934	TTGATGTCCACACCGAATGC	CGAAAAGTAAAGCCAGGTACGG
	LOC108981203	AATGGTGGGAGTTTGTGTGC	TGGCCAGTCAACAAGCAATC
	LOC109002086	GCTAGAGTGCAAGGCTTTTAGC	AATGGTTGGTCGCGTCTTTG
	LOC109016564	TCCCCCATTTCAAGGCACTC	AAAGCAAAGCCAAGCCAAGC
	LOC109005209	AAAGCACACTGGTCACTGAG	TTCTTCGCTTGTGGTCTCAC
C. gloeosporioides	*β*-tubulin	CACTCTCTCCGTCCACCAG	CGGACATAACAGCAGAGACCA
	GCG54_00008766	CCTCAACGACGAGATCAACAAG	CTTGCTCGTCGTATATCTTGCC
	GCG54_00013010	ATCAAGGCCGTCACCAAGTC	TTCTTGCCCTCGAACTCCTTG
	GCG54_00011250	TACGCCGATTATCCTTTCACCT	GGATTGGTTTCTTCCGCTCT
	GCG54_00007763	ATATGCAGGTCTTGTTCGTTC	TCCACCGCTGACAATGTTTCG
	GCG54_00014461	ATCAACCGCACCTACCCTC	CGCCTTGTTTCTCTCACCGAT
	GCG54_00010327	GCGTTCGCCGATAACATGAC	AGGGACCACTACAGCTCCTT
	GCG54_00012294	GGACTAAGGACCCTAACACGA	AAGAGAAACCAGCTCGCAAG
	GCG54_00007391	TTCCTTACCAACCTGTGGCTT	CGCCGATCCAGTCATACTCG
	GCG54_00015103	ACTGCGTCTGTCCGAAACAT	TGAAAGGAGTGCGAGGTTCC
	GCG54_00003598	GTTGGAAGAACAGCGAGGGA	GTGTATCTGGTCTGCGTGCT
B. velezensis	16S rRNA	CATCATGCCCCTTATGACCTG	ATTACTAGCGATTCCAGCTTC
	AAV34_RS08320	TCACGCAGATCATTCAGGT	CCATTTCAGTCATAAGCGACA
	AAV34_RS06000	TTTCTTATTCCCGAACACCAC	GCCGTTTTCAGACAGTGACA
	mprF	CCGCTCTGTTTATTATCGC	CAATAATGGCCGTCATCGTG
	srfAB	AGCCTCTTAAATCATTTGGTC	ATTGAAATCAAAGCTCGTCT
	AAV34_RS00945	CTGCTGCTTCTTGTCACTGG	ACGTGCAGTTGAACATATCTCC
	AAV34_RS17985	CCTGATCTTCGTCATCGCTCT	CCGGCTCTTCATTTGAGACCA
	AAV34_RS08265	AACATCACGCACAATGACGAA	GCTCCCATCTCATAAAGGGTT
	AAV34_RS08280	ATTCAATCTTGGCTGAAGTCG	TTTGTCAGTACTTGCGCCAGA
	comER	TATTCAAACGCTGTTCACTCA	CGCTGAACGAGATAACTCA
	AAV34_RS08275	TCCAATGTATATCTCGCTCC	CTCCATTGTCACGTAAACGA

Differential gene expression profiling in tripartite walnut-*C. gloeosporioides*-*B. velezensis* interactions

Walnut transcriptomes revealed 7,860 (B vs. C), 3,677 (T vs. C), 888(TB vs. B), 5,587 (TB vs. T), and 7,345 (TB vs. C) differentially expressed genes (DEGs) across comparison groups ($p < 0.05$, FDR < 0.01; Fig. 1a). Notably, *C. gloeosporioides* inoculation under *B. velezensis* pretreatment (TB vs. B) induced 75.8% fewer DEGs than single-pathogen inoculation (T vs. C). Co-inoculation (TB vs. C) generated 6.5% fewer DEGs than *B. velezensis* mono-inoculation (B vs. C), but 99.8% more than *C. gloeosporioides* mono-inoculation (T vs. C). These results indicate that walnuts exhibit different transcriptional responses to the treatments of *B. velezensis* and *C. gloeosporioides*.

For *C. gloeosporioides*, there were 92 and 749 differentially expressed genes in the comparison groups of TB vs. T and TB vs. B, respectively (Fig. 1b). In both comparison groups, the number of up-regulated differentially expressed genes was greater than that of down-regulated

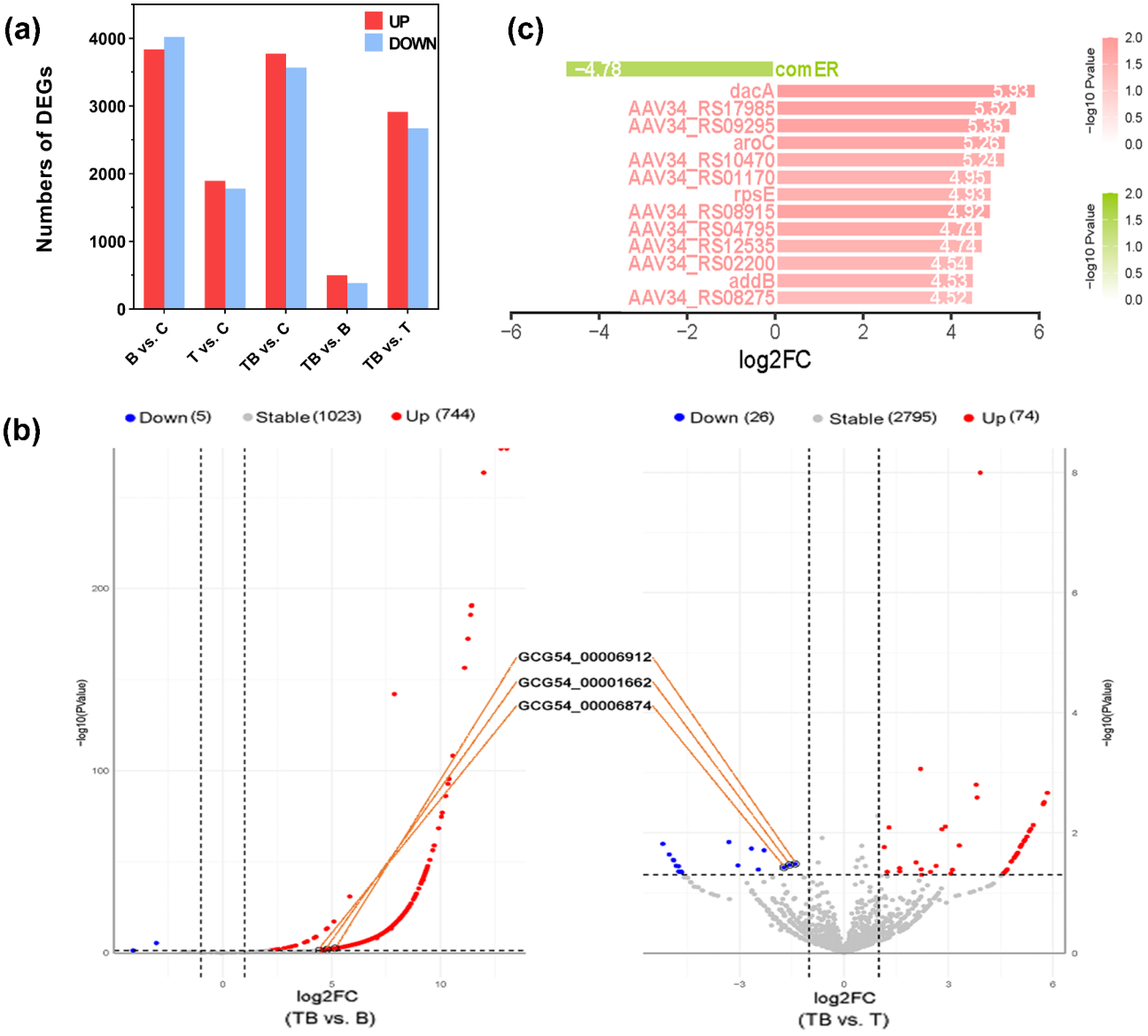

Fig. 1 Analysis of differentially expressed genes (DEGs) in the three-way interaction system. (**a**). The number of up and down regulated DEGs of walnuts in the comparison groups of B vs. C、T vs. C、TB vs. B、TB vs. T and TB vs. C. (**b**). Volcano plot of DEGs of *Colletotrichum gloeosporioides*. The left and right sides are the comparison groups of TB vs. B and TB vs. T respectively. The x-axis represents the $\log_2$FoldChange, and the y-axis represents the -$\log_{10}$PValue. The gray dots represent the genes without differential expression, the blue dots represent the genes with down-regulated differential expression, and the red dots represent the genes with up-regulated differential expression. (**c**). Bar chart of specific DEGs in the TB vs. T group of *Bacillus velezensis*. Pink indicates up-regulated expression, and green indicates down-regulated expression. The length of the bars represents the magnitude of the difference ($\log_2$FoldChange), and the shade of the color represents the degree of significance of the difference (-$\log_{10}$P-Value)

ones. Among them, three genes were up-regulated in the TB vs. B comparison group but down-regulated in the TB vs. T comparison group, suggesting *B. velezensis*-mediated transcriptional interference of *C. gloeosporioides*.

For *B. velezensis*, there were a total of 78 up-regulated differentially expressed genes and 1 down-regulated differentially expressed gene in the comparison groups of TB vs. B and TB vs. T, and 83 up-regulated differentially expressed genes in the comparison group of B vs. T. Under the influence of *C. gloeosporioides*, *B. velezensis* produced 14 unique differentially expressed genes (the differentially expressed genes in TB vs. T excluding those identical to those in the B vs. T comparison group). Notably, the comER gene was significantly downregulated (log_2FC = -4.78), while 13 genes showed > 4.5-fold upregulation (Fig. 1c). This suggests that the transcriptional response of *B. velezensis* is influenced by *C. gloeosporioides*.

Functional annotation of walnut DEGs through GO and KEGG enrichment analyses

To characterize the biological significance of walnut differentially expressed genes (DEGs) across experimental groups, Gene Ontology (GO) and Kyoto Encyclopedia of Genes and Genomes (KEGG) enrichment analyses were performed. Significantly enriched terms ($p < 0.05$) were identified in three GO categories: biological processes (BP), molecular functions (MF), and cellular components (CC). The twenty most enriched terms per comparison group were visually prioritized in subsequent analyses (Fig. 2). Notably, *B. velezensis* mono-inoculation (B vs. C) and co-inoculation (TB vs. C) shared identical top 20 GO terms, whereas *C. gloeosporioides* mono-inoculation (T vs. C) uniquely exhibited cellular protein-containing complex assembly (GO:0034622) as a distinctive BP term (Fig. 2a, c). Intriguingly, pathogen-challenged walnuts with subsequent biocontrol inoculation (TB vs. B) demonstrated divergent enrichment patterns, top BP terms associated with nucleobase-containing small molecule metabolic process (GO:0055086), drug metabolic process (GO:0017144), and amino acid biosynthetic and metabolic process (GO:0006520, GO:1901605, and GO:0008652) (Fig. 2d). Comparative analysis revealed treatment-specific responses, co-inoculation under pathogen pressure (TB vs. T) showed three unique BP terms versus other groups (B vs. C & TB vs. C): Protein localization to organelles (GO:0033365), translation (GO:0006412), and mRNA processing (GO:0006397) (Fig. 2a, c, e). These findings collectively suggest that biocontrol inoculation reprograms host biological processes during pathogen infection, particularly enhancing biological processes.

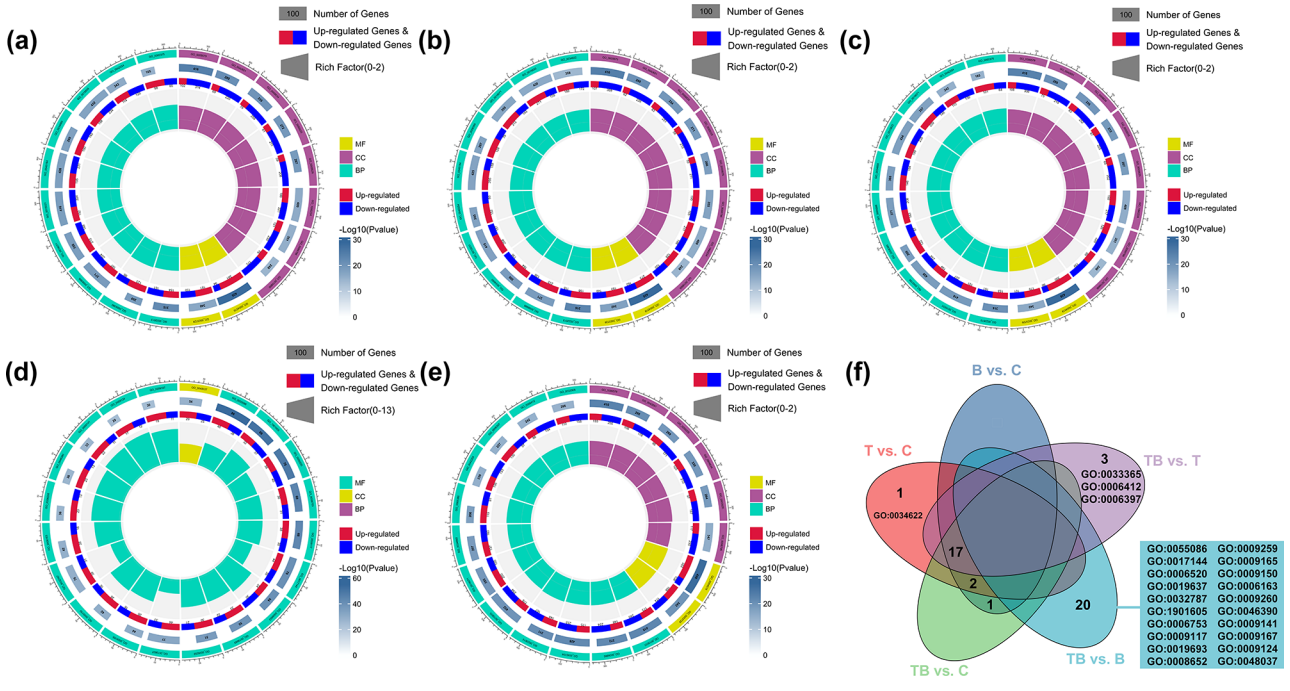

Fig. 2 Gene Ontology (GO) enrichment analysis of walnut DGEs. (a-e). Enrichment circle plots for B vs. C (**a**)、T vs. C (**b**)、TB vs. C (**c**)、TB vs. B (**d**)、TB vs. T (**e**). (**f**). Veen diagram of GO terms annotated in each comparison group. The outer circle displays the GO term and its corresponding category. Green represents biological_process (BP), purple represents cellular_component (CC), and yellow represents molecular_function (MF). The number below represents the number of genes belonging to this GO term in the input gene file. The color indicates the magnitude of -log_{10}(Pvalue). The darker the color, the larger this value is. The second layer shows the expression of each gene in this GO term. Red indicates up-regulation, and blue indicates down-regulation. The innermost layer represents the enrichment score of this GO term

KEGG functional annotation of differentially expressed genes (DEGs) across comparison groups identified conserved and divergent pathway activation patterns ($p < 0.05$). Two core pathways were universally enriched in all groups: plant hormone signal transduction pathway(ko04075) and ribosome pathway(ko03010) (Fig. 3). Contrastive analysis revealed treatment-specific signatures, *B. velezensis* mono-inoculation (B vs. C) uniquely activated: Biosynthesis of amino acids (ko01230) and mRNA surveillance pathway (ko03015); Co-inoculation (TB vs. C) exhibited exclusive enrichment in: Carbon fixation by Calvin cycle (ko00710) and Proteasome (ko03050) (Fig. 3a, c). Compared with the treatment with *C. gloeosporioides* (T vs. C), under the treatment of *B. velezensis*, the co-treatment with *C. gloeosporioides* and *B. velezensis* (TB vs. B) had fewer differentially expressed genes annotated to the same metabolic pathway (Fig. 3b, d). Co-inoculation with pathogen priming (TB vs. T) versus *B. velezensis* mono-inoculation (B vs. C) activated four novel pathways: Zeatin biosynthesis (ko00908), Protein processing in endoplasmic reticulum (ko04141), Nucleotide excision repair (ko03420), and Circadian rhythm (ko04712) (Fig. 3a, e). These results indicate that biocontrol bacteria can induce different metabolic pathways in plants to resist pathogens when the plants are infected with pathogens, preferentially enhancing secondary metabolite synthesis and stress-responsive proteostasis during biotic challenge.

Major KEGG pathways of DEGs in walnut

In the plant-pathogen interaction pathway (Fig. 4a), a majority of disease-resistance proteins showed upregulation across all comparison groups (fold changes: 1.01 ~ 9.86). The fold changes of upregulated genes LOC118349226 (RPS2), LOC108983266 (RPS2), LOC109001409 (RPM1), and LOC109008319 (RPM1) were significantly higher in TB vs. C than in T vs. C. Additionally, LOC109006418 (MEKK1) and LOC109004780 (PBS1) exhibited significant upregulation in B vs. C, TB vs. C, and TB vs. T. The pathogenesis-related proteins LOC109002956/LOC109020655 (PR1) were markedly upregulated in T vs. C (fold changes: 1.70/6.43) but downregulated in TB vs. T (fold changes: 2.87/5.56). Collectively, these findings indicate that walnut plants activate the expression of disease resistance-associated genesin response to pathogen-derived signals and biocontrol bacterial stimuli.

In the plant hormone signal transduction pathway (Fig. 4b), differentially expressed genes were predominantly associated with hormones (abscisic acid, auxin, ethylene, gibberellin, etc.), transcription factors, and two-component regulatory response factors. Within phenylalanine metabolism related to disease resistance, LOC109014782 (PR-1) exhibited a 7.62-fold upregulation in B vs. C but a 9.79-fold downregulation in TB vs. B. Regarding carotenoid biosynthesis linked to stomatal closure, all genes except the abscisic acid receptor genes LOC109010128 (PYL8) and LOC109009683

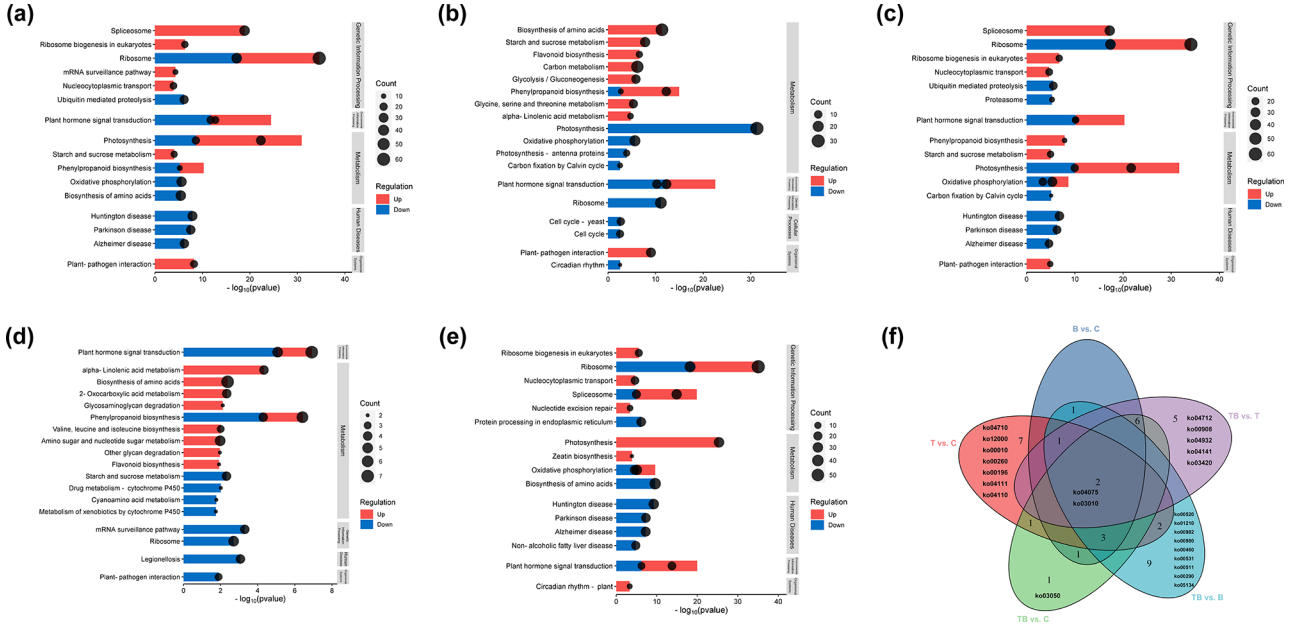

Fig. 3 Kyoto Encyclopedia of Genes and Genomes (KEGG) pathway enrichment analysis of walnut DEGs. (a-e). Dot-line plots for B vs. C (**a**), T vs. C (**b**), TB vs. C (**c**), TB vs. B (**d**), and TB vs. T (**e**). (**f**). Venn diagram of KEGG pathways annotated in each comparison group. The bar represents the magnitude of the p-value. The longer the bar, the smaller the p-value. The dot represents the number of genes. The larger the dot, the greater the number of genes. The color of the bar indicates the gene expression status. Red indicates up-regulation, and blue indicates down-regulation. The right side represents the classification type of KEGG pathway

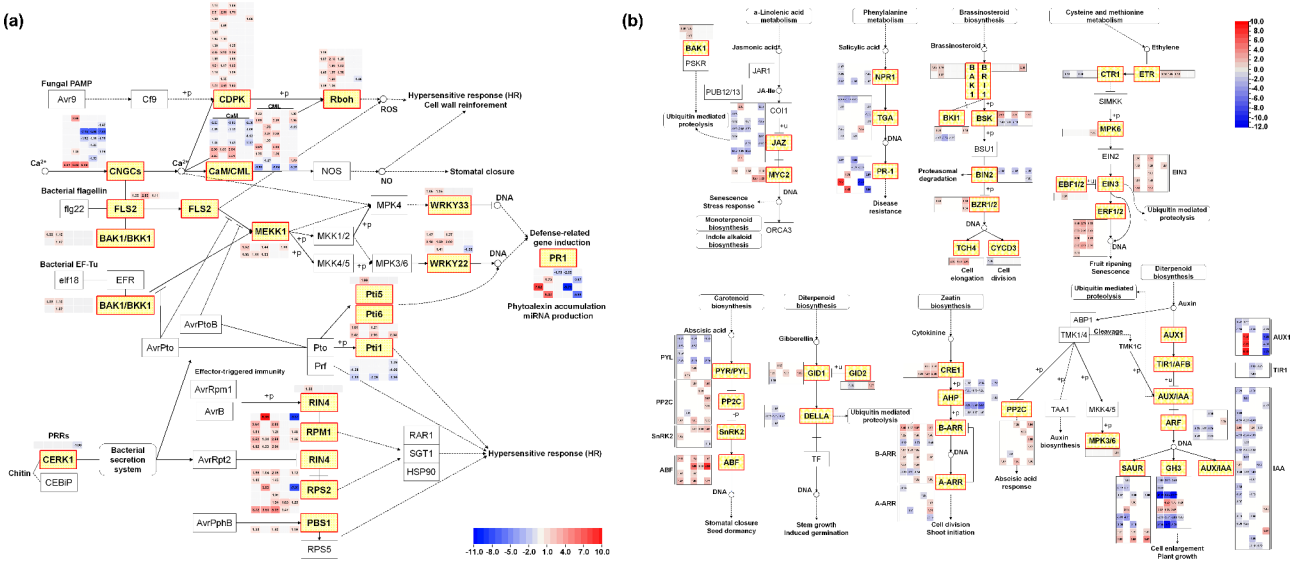

Fig. 4 Kyoto Encyclopedia of Genes and Genomes (KEGG) key pathway diagram of walnut DEGs. (**a**). Plant-pathogen interaction; (**b**). Plant hormone signal transduction. The heatmap shows the $\log_2$FoldChange values of the comparison groups B vs. C, T vs. C, TB vs. C, TB vs. B, and TB vs. T from left to right. The gray blocks indicate that the differences in this comparison group are not significant. The color of the heatmap changes from blue to red, representing the change of the fold - difference from small to large. The square with a red - framed line and a yellow background represents the differentially expressed genes annotated on this pathway

(PYL2) were downregulated, with the latter showing modest upregulations of 1.20- and 1.46-fold, respectively. ABF proteins displayed significantly induction, particularly LOC108985710 (ABF5) which showed an 8.24-fold upregulation in TB vs. T. In α-linolenic acid metabolism associated with stress response, MYC2 was consistently upregulated (fold changes: 1.13 ~ 3.23) across all comparisons except T vs. C. The PP2C gene involved in abscisic acid signaling was downregulated 1.18-fold in T vs. C but upregulated (1.07 ~ 2.08-fold) in other groups. Cell expansion-related genes LOC109011353 (SAUR36) and LOC118348389 (SAUR36) demonstrated 1.25- to 2.58-fold upregulations in B vs. C, TB vs. C, and TB vs. T. Auxin biosynthesis genes (LOC10899306, LOC108999650, LOC109015024) were sharply induced (7.87 ~ 9.00-fold) in T vs. C yet suppressed (1.29 ~ 7.62-fold) in TB vs. T.

Transcriptome functional analysis of *C. gloeosporioides*

To identify the genes associated with the functions roles of *C. gloeosporioides* in the three-way interaction system, we performed transcriptomic functional profiling of the pathogen (Fig. 5a). The results of the GO enrichment analysis showed that in the comparison group TB vs. T, the top three terms enriched for the up-regulated differentially expressed genes in the biological process category were chromatin assembly or disassembly (GO:0006333), nucleosome assembly (GO:0006334), and chromatin assembly (GO:0031497); in the molecular function category, the top three enriched terms were binding (GO:0005488), structural constituent of ribosome (GO:0003735), and structural molecule activity (GO:0005198). In the comparison group TB vs. B, the top three terms enriched for the up-regulated differentially expressed genes in the molecular function category were ion binding (GO:0043167), binding (GO:0005488), and Ras GTPase binding (GO:0017016); in the biological process category, the top three enriched terms were protein acetylation (GO:0006473), chromatin assembly or disassembly (GO:0006333), and nucleosome assembly (GO:0006334). Notably, TB vs. T exhibited fewer genes enriched in ion binding and general binding terms compared to TB vs. B, suggesting that colonization of walnut hosts by *B. velezensis* modulates molecular functions in *C. gloeosporioides*.

KEGG functional annotation was performed on the differentially expressed genes in each comparison group. The top 15 pathways of the up-regulated differentially expressed genes in the TB vs. B comparison group, as well as all the pathways annotated by the upregulated and downregulated differentially expressed genes in the TB vs. T comparison group, were selected for subsequent analysis (Fig. 5b). The downregulated differentially expressed genes in the TB vs. T comparison group were annotated to the Synaptic vesicle cycle pathway (ko04721). In the TB vs. T comparison group, the main upregulated genes enriched pathways included Ribosome (ko03010), Antigen processing and presentation (ko04612), and Ribosome biogenesis in eukaryotes (ko03008). Compared with the TB vs. B comparison group, Ribosome (ko03010), Antigen processing and presentation (ko04612), Phagosome (ko04145), and

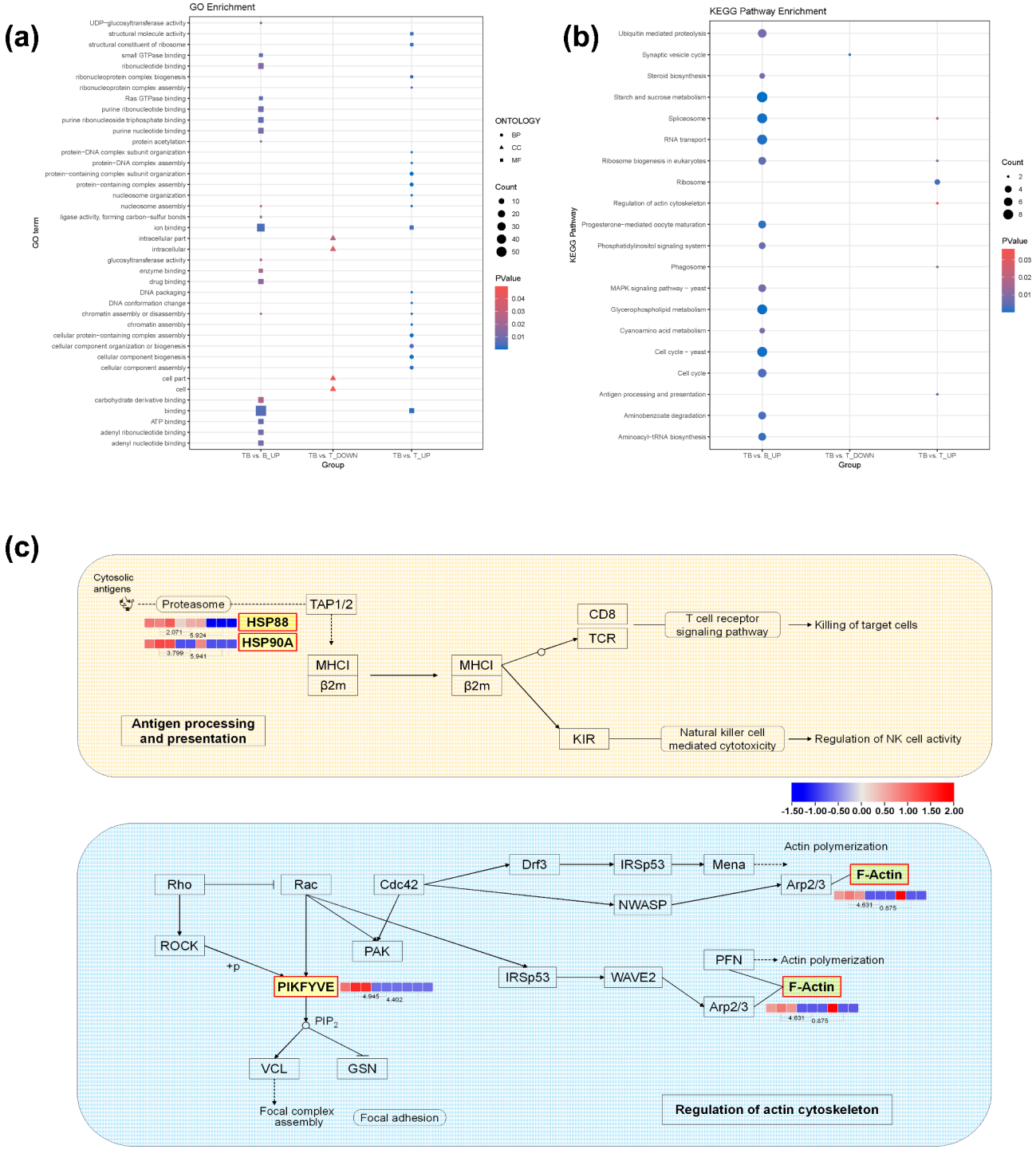

Fig. 5 Gene Ontology (GO) and Kyoto Encyclopedia of Genes and Genomes (KEGG) enrichment functional analysis of *Colletotrichum gloeosporioides* DEGs. (**a**). GO enrichment analysis bubble chart. Select the top 20 GO terms annotated with up-regulated differentially expressed genes in the TB vs. B and TB vs. T comparison groups, and all GO terms annotated with down-regulated differentially expressed genes in the TB vs. T comparison group. The P-value is shown from small to large, ranging from blue to red. The size of the bubble represents the size of the Count value. The bubble shapes, circle, triangle, and square, represent Biological process, Cellular component, and Molecular function respectively. (**b**). KEGG pathway enrichment analysis bubble chart. Select the top 20 KEGG pathways annotated with up-regulated differentially expressed genes in the TB vs. B comparison group, and all KEGG pathways annotated with up-regulated and down-regulated differentially expressed genes in the TB vs. T comparison group. The P-value is shown from small to large, ranging from blue to red. The size of the bubble represents the size of the Count value

Regulation of actin cytoskeleton (ko04810) were unique to the TB vs. T comparison group. Similarly, the enrichment degrees of Ribosome biogenesis in eukaryotes (ko03008) and Spliceosome (ko03040), which were also enriched, were significantly lower in the TB vs. T comparison group than in the TB vs. B comparison group.

Based on the functional annotation and KEGG enrichment analysis, attention was focused on the Antigen processing and presentation pathway and the Regulation of actin cytoskeleton pathway that appeared exclusively in the TB vs. T comparison group (Fig. 5c). The differentially expressed genes HSP88, HSP90A, PIKFYVE, and F-Actin all exhibited higher expression levels in the TB treatment group. However, the differentially expressed fold changes of the two differentially expressed genes (PIKFYVE and F-Actin) annotated in the Regulation of actin cytoskeleton pathway were greater.

Transcriptome functional analysis of *B. velezensis*

To identify the genes involved in the functions of *B. velezensis* in the tripartite system, a functional analysis of the transcriptome of the biocontrol bacterium was conducted. According to the results of the GO enrichment analysis (Fig. 6a), in the biological process category, the sulfur compound biosynthetic process (GO:0044272) was enriched with two up-regulated differentially expressed genes in the TB vs. T comparison group, and the L-proline biosynthetic process (GO:0055129) was enriched with one down-regulated differentially expressed gene in the TB vs. B comparison group. In the molecular function category, transmembrane transporter activity (GO:0022857), transporter activity (GO:0005215), transferase activity, transferring acyl groups (GO:0016746), and catalytic activity, acting on RNA (GO:0140098) were enriched with 8, 8, 4, and 2 up-regulated differentially expressed genes, respectively, in the TB vs. T comparison group. In the TB vs. B comparison group, catalytic activity (GO:0003824) and phosphopantetheine binding (GO:0031177) were each enriched with one up-regulated differentially expressed gene, and pyrroline-5-carboxylate reductase activity (GO:0004735) was enriched with one down-regulated differentially expressed gene. In the cellular component category, the cytoplasm (GO:0005737) was enriched with one down-regulated differentially expressed gene. Under the influence of *C. gloeosporioides*, *B. velezensis* showed differences in biological processes, molecular functions, and cellular components. Among them, the molecular function category was enriched with the most differentially expressed genes, indicating that in the interaction between *B. velezensis* and *C. gloeosporioides*, more molecular functions related to transmembrane transporter activity and transporter activity are induced.

KEGG functional annotation was performed on the differentially expressed genes across all comparison group (Fig. 6b). In the TB vs. T comparison group, the DEGs predominantly classified under the primary KEGG category of Metabolism. Specifically, these genes mapped to five metabolic pathways: Biosynthesis of amino acids (5 genes), Carbon metabolism (4 genes), Citrate cycle (TCA cycle; 3 genes), Glyoxylate and dicarboxylate metabolism (3 genes), and 2-Oxocarboxylic acid metabolism (2 genes).

GO functional annotation combined with KEGG enrichment analysis revealed that DEGs were primarily associated with four key pathways: Biosynthesis of amino acids, Citrate cycle (TCA cycle), Glyoxylate and dicarboxylate metabolism, and Carbon metabolism (Fig. 6c). Among them, while metE and aroC were exclusively involved in amino acid biosynthesis, other DEGs exhibited pleiotropic regulatory roles across multiple pathways. Furthermore, expression levels of aroC and rpe—genes participating in both amino acid biosynthesis and carbon metabolism—were significantly upregulated in the TB group compared to controls.

Identification of candidate genes based on the weighted gene Co-expression network (WGCNA)

A weighted gene co-expression network of *B. velezensis* was constructed using WGCNA. To establish a scale-free network (scale-free topology fit index $R^2 \geq 0.8$), the soft threshold power (β) was set to 20. Eleven modules were identified and displayed in different colors (Fig. S2a). We analyzed module-trait correlations and visualized them in a heatmap (Fig. 7a). The MEred module showed a significantly positive correlation with the co-inoculation treatment of *C. gloeosporioides* and *B. velezensis* ($r = 0.78$, $p = 0.01$), but a non-significant correlation with *B. velezensis* single inoculation. In contrast, the MEblue module was strongly positively correlated with *B. velezensis* single inoculation ($r = 0.97$, $p = 1e\text{-}05$). Using the CytoHubba plugin in Cytoscape, we screened hub genes from both modules. The interaction network of the top 15 candidate genes identified by the MCC algorithm is shown in the Fig. 7b. Among the candidate genes obtained from the MEred module, five gene (AAV34_RS19635, AAV34_RS04795, addB, bioA, and AAV34_RS08275) were differentially expressed genes.

For *C. gloeosporioides*, a scale-free network (scale-free topology fit index $R^2 \geq 0.8$) was established by setting the soft threshold to $\beta = 20$. Seventeen modules were identified and displayed in different colors (Fig. S2b). After analyzing the correlations between the modules and different treatments, a heatmap was generated (Fig. 7c). The MEturquoise module showed a significant positive correlation with *C. gloeosporioides* single inoculation ($r = 0.99$, $p = 8e\text{-}08$) and a correlation but non-significant with the co-inoculation treatment of *C. gloeosporioides* and *B. velezensis*. The MEbrown module was positively

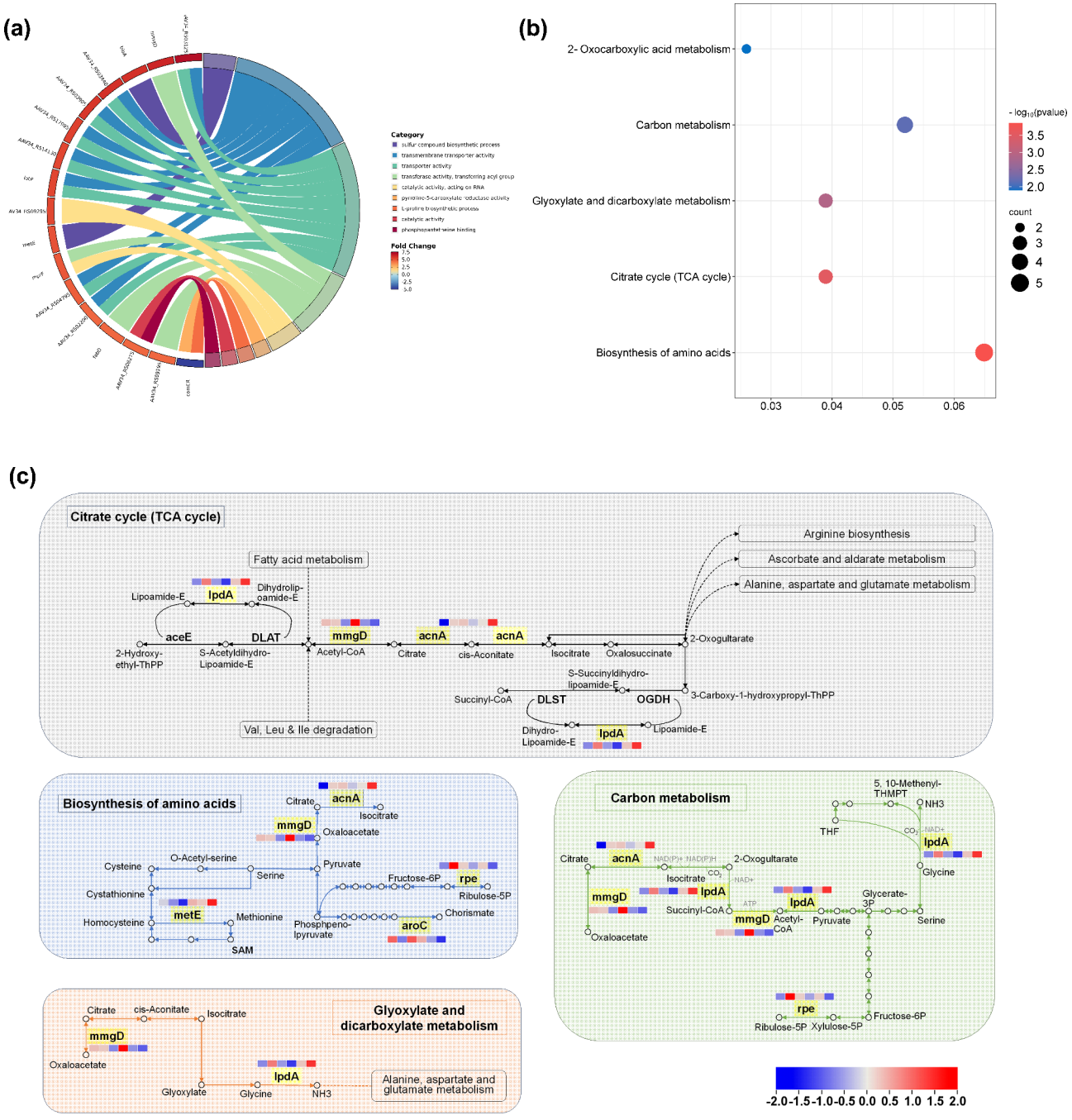

Fig. 6 Gene Ontology (GO) and Kyoto Encyclopedia of Genes and Genomes (KEGG) enrichment functional analysis of *Bacillus velezensis* DEGs. (**a**). GO enrichment analysis chord diagram. Chords of different colors represent the correspondence between differentially expressed genes and GO terms. The legend on the right explains the GO terms corresponding to different colors. The squares next to the gene names, ranging from blue to red, indicate the magnitude of the difference (log_2FoldChange). (**b**). KEGG pathway enrichment analysis bubble chart. The x-axis represents the GeneRatio, and the y-axis lists different metabolic pathways. The size of the bubble indicates the number of genes in the pathway, and the color of the bubble represents the p-value. The color gradient ranges from blue (lower p-value) to red (higher p-value)

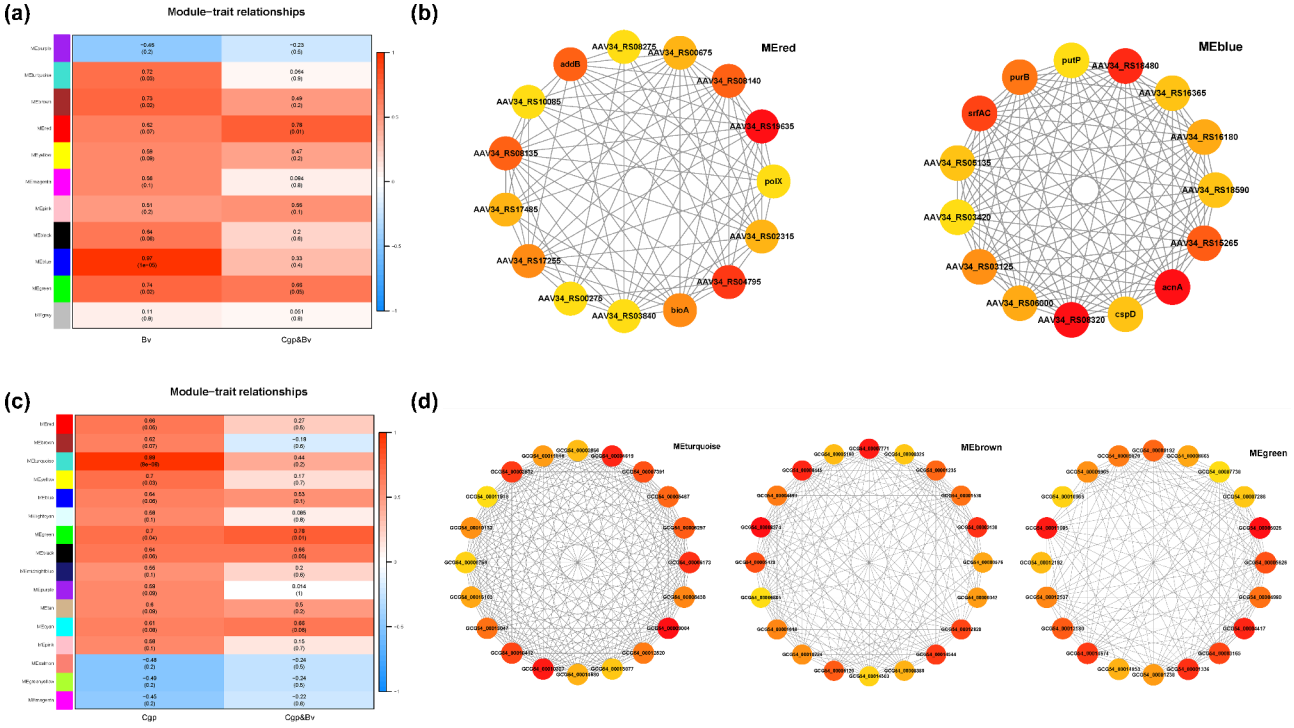

Fig. 7 Weighted gene co-expression network analysis (WGCNA) modules analysis and interaction network diagram of candidate genes in key modules. (**a**). Heatmap of the WGCNA module correlations with inoculate Bv and inoculate Cgp & Bv traits of *Bacillus velezensis*. (**b**). Interaction network diagram of candidate genes in MEred and MEblue modules of *Bacillus velezensis*. (**c**). Heatmap of the WGCNA module correlations with inoculate Cgp and inoculate Cgp & Bv traits of *Colletotrichum gloeosporioides*. (**d**). Interaction network diagram of candidate genes in MEturquoise, MEbrown and MEgreen modules of *Colletotrichum gloeosporioides*

correlated with the *C. gloeosporioides*-only treatment but negatively correlated with the co-inoculation treatment. The MEgreen module exhibited significant positive correlation with the co-inoculation treatment ($r = 0.78$, $p = 0.01$) and the *C. gloeosporioides* single inoculation ($r = 0.7$, $p = 0.04$). The interaction network of the top 20 candidate genes (identified via the MCC algorithm) is shown in the Fig. 7d.

Candidate genes based on the protein-protein interaction (PPI) network

The interaction network analysis of differentially expressed proteins within key modules utilized interaction data from the STRING database, with visualization of the PPI network achieved via Cytoscape (v3.10.3). For *B. velezensis*, only two pairs of interacting proteins were annotated in the MEred module, which was insufficient for constructing a reliable PPI network required for MCC calculation. In contrast, the interaction network analysis was conducted for the MEblue module (Fig. S3a), and the top 10 candidate genes were identified via MCC scoring using the CytoHubba plugin in Cytoscape (Fig. 8a).

Similarly, the interaction network analysis of the differentially expressed gene proteins within the MEturquoise, MEbrown, and MEgreen modules of *C. gloeosporioides* was performed (Fig. S3b, c, d), and the top 20 candidate genes were ranked by MCC scores using CytoHubba (Fig. 8b, c, d).

Identification of hub genes based on WGCNA and PPI

For *B. velezensis*, the results of WGCNA and PPI analyses were used to identify key candidate genes sets using the CytoHubba plugin in Cytoscape softwarem, respectively. The hub genes were determined by identifying the overlapping genes across these gene sets (Fig. 9a). The final hub genes, srfAC and purB (both differentially expressed), were selected for further analysis.

For *C. gloeosporioides*, the top 20 key candidate genes sets were also identified using the CytoHubba plugin in Cytoscape software. The hub genes were determined by identifying the overlapping genes across these gene sets (Fig. 9b, c, d). Four, three, and two hub genes were derived from the MEturquoise, MEbrown, and MEgreen modules, respectively (Table S2).

Validation of RNA-Seq sequencing data by real-time quantitative PCR (qRT-PCR)

To validate the RNA-Seq data, randomly selected differentially expressed genes (DEGs) were analyzed by qRT-PCR. The qRT-PCR expression patterns of these genes

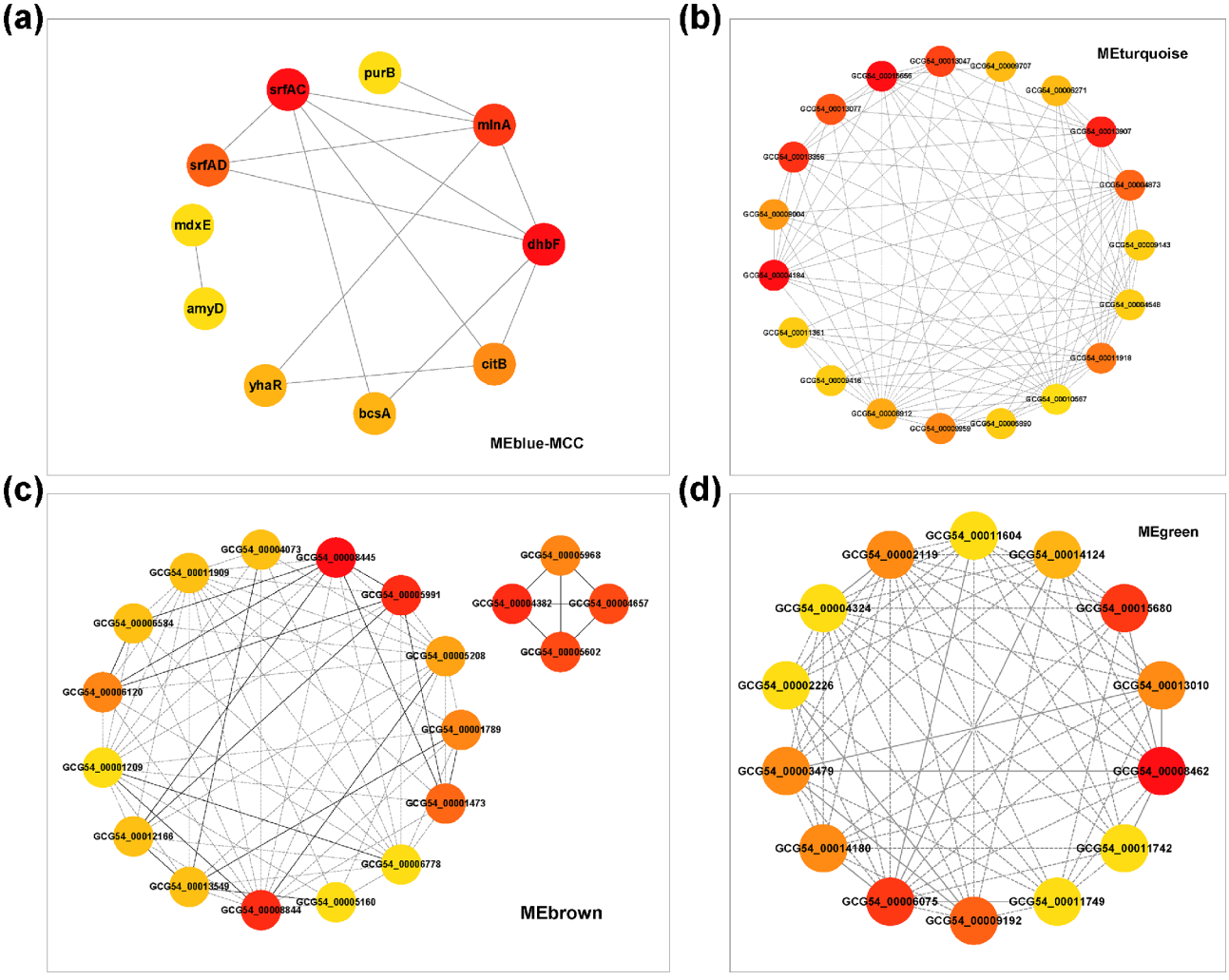

Fig. 8 Interaction network diagram of candidate genes whtin PPI network analysis in key modules. (**a**). Interaction network diagram of candidate genes within PPI network analysis in MEblue modules of *Bacillus velezensis*. (**b**)-(**d**). Interaction network diagram of candidate genes within PPI network analysis in MEturquoise, MEbrown and MEgreen modules of *Colletotrichum gloeosporioides*

showed strong agreement with the RNA-Seq results (Fig. 10), with consistency rate of 96% in walnuts and 100% in both *B. velezensis* and *C. gloeosporioides*. These findings demonstrate that the transcriptional changes observed in all three species are robust and corroborate the reliability of the RNA-Seq dataset.

Discussion

Existing studies on plant-microbe interactions predominantly focus on pairwise relationships between plants and pathogens/biocontrol agents or between pathogens and biocontrol bacteria. To advance this field, our study examines transcriptional responses within the tripartite "Walnut-*Colletotrichum gloeosporioides-Bacillus velezensis* " system through a three-way interaction network. Through integrative analysis combining WGCNA and PPI network approaches, we identified GCG54_00005160 (CGS) in the MEbrown module (positive correlation with *C. gloeosporioides* single inoculation and negative correlation with co-inoculation with *C. gloeosporioides* and *B. velezensis*) as a hub gene (Fig. 9c). Notably, CGS encodes a key enzyme in the cysteine-methionine biosynthesis pathway, which has established roles in fungal pathogenesis [18, 19]. It suggests *B. velezensis* modulates transcriptional programming in *C. gloeosporioides* within the tripartite system. In the TB vs. T comparison group of *C. gloeosporioides*, the differentially expressed genes PIKFYVE and F-Actin in the regulation of actin cytoskeleton pathway were significantly upregulated (Fig. 5c). Concurrently, synaptic vesicle cycle components AVT1 (GCG54_00001435) and VHA-A (GCG54_00006572) showed marked downregulation (Fig. 5b). Given that cytoskeletal remodeling coordinates critical infection processes in phytopathogens - including hyphal morphogenesis, appressorium formation, and host colonization [20], the observed actin upregulation implies *B. velezensis*

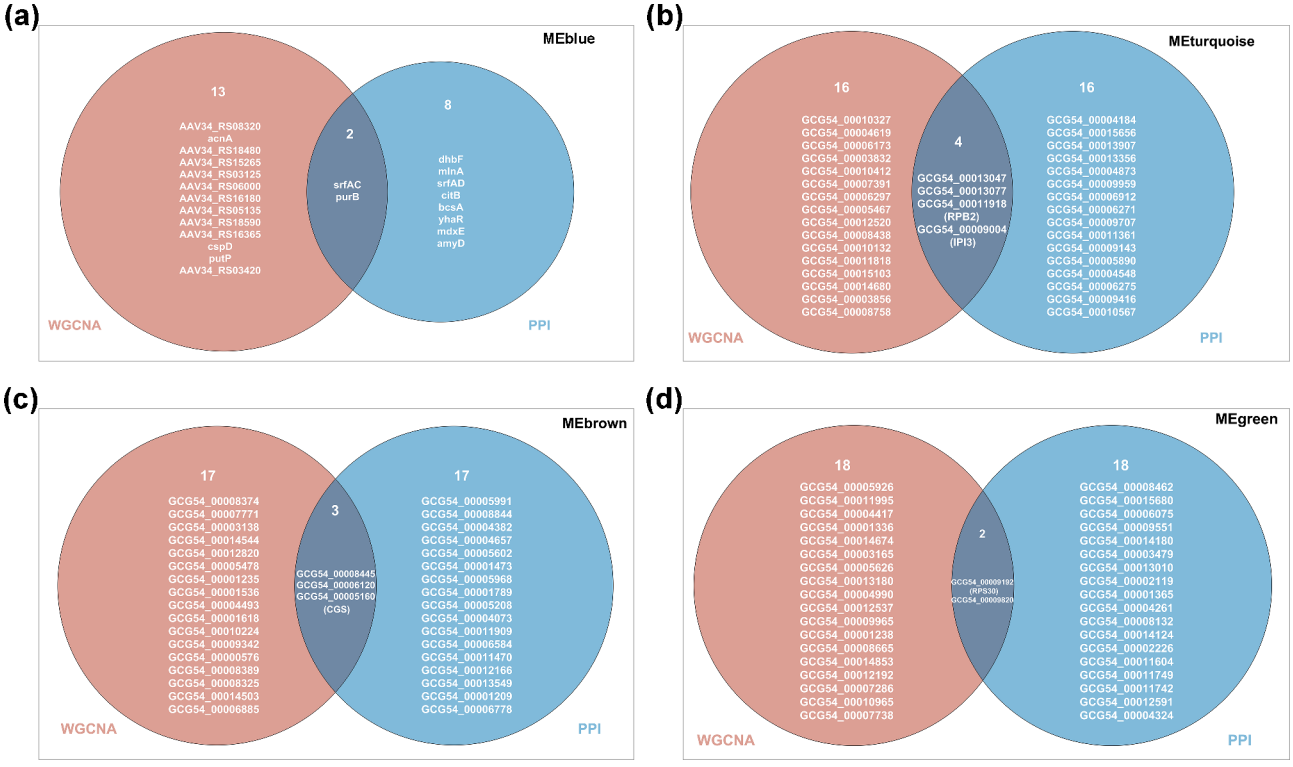

Fig. 9 Veen diagram of candidate genes from WGCNA and PPI network analysis. (**a**). Overlap of candidate gene sets in MEblue modules of *Bacillus velezensis*. (**b**)-(**d**). Overlap of candidate gene sets in MEturquoise, MEbrown and MEgreen modules of *Colletotrichum gloeosporioides*

may provoke cytoskeletal dynamics in *C. gloeosporioides* during interaction. This interpretation aligns with established roles of F-actin in fungal adhesion and infection-related cytoskeletal reorganization [21, 22]. Compared with the single infection of walnuts by *C. gloeosporioides*, the biocontrol bacterium *B. velezensis* significantly upregulated the actin expression of *C. gloeosporioides*, indicating that the biocontrol bacterium can stimulate the dynamic regulation of the cytoskeleton of the pathogen. Meanwhile, our results also show that the biocontrol bacterium *B. velezensis* inhibits the synaptic vesicle cycle of *C. gloeosporioides*. Considering that synaptic vesicles mediate transport of virulence factors such as extracellular proteases and adhesion molecules [23–25], this dual regulatory effect of simultaneous induction of cytoskeletal stress and impairment of virulence factor delivery maybe is a novel biocontrol mechanism. To our knowledge, the changes in these pathways are rarely mentioned in *Bacillus*-mediated biocontrol, providing a new perspective for future research.

Overall, *B. velezensis* is less affected by the transcriptional response of *C. gloeosporioides* in the tripartite system. Biofilms, which are critical for bacterial adhesion and cell protection, are regulated in *Bacillus* spp. by comER through the transcription factor Spo0A modulation [26, 27]. Among the unique differentially expressed genes in the TB vs. T comparison group, comER was significantly down-regulated ($p < 0.05$, Fig. 1c), indicating that *C. gloeosporioides* may inhibit *B. velezensis* growth by disrupting biofilm formation. Furthermore, the significantly up-regulated genes aroC and metE are involved in the amino acid biosynthesis pathway (Figs. 1c and 6c). AroC, a key enzyme in the shikimate pathway, contributes to antibacterial compound production in *Brevibacillus brevis* [28], while metE, an S-thioallylated protein, confers resistance to allicin and DAS4 in *Bacillus subtilis* [29]. Additionally, dacA plays an important role in the synthesis and stabilization of peptidoglycan in the bacterial cell wall, and it's may enhance cell membrane permeability, facilitating extracellular protein secretion [30]. Combined WGCNA and PPI analyses identified srfAC and acnA as hub genes in *B. velezensis* (Fig. 9a), are crucial for the biosynthesis of antibacterial compounds in *Bacillus*. Specifically, srfAC is a gene positively regulated by iron, promotes antibacterial biosynthesis and pathogen competition [31–33]. these results suggest that *B. velezensis* counteracts *C. gloeosporioides* stress via enhanced antimicrobial production and secretion in the tripartite system.

When plants are colonized by foreign microorganisms, they activate a series of defense responses. Previous studies have demonstrated that *B. velezensis* promotes plant growth through secondary metabolites and secretes antimicrobial compounds to inhibit pathogen invasion

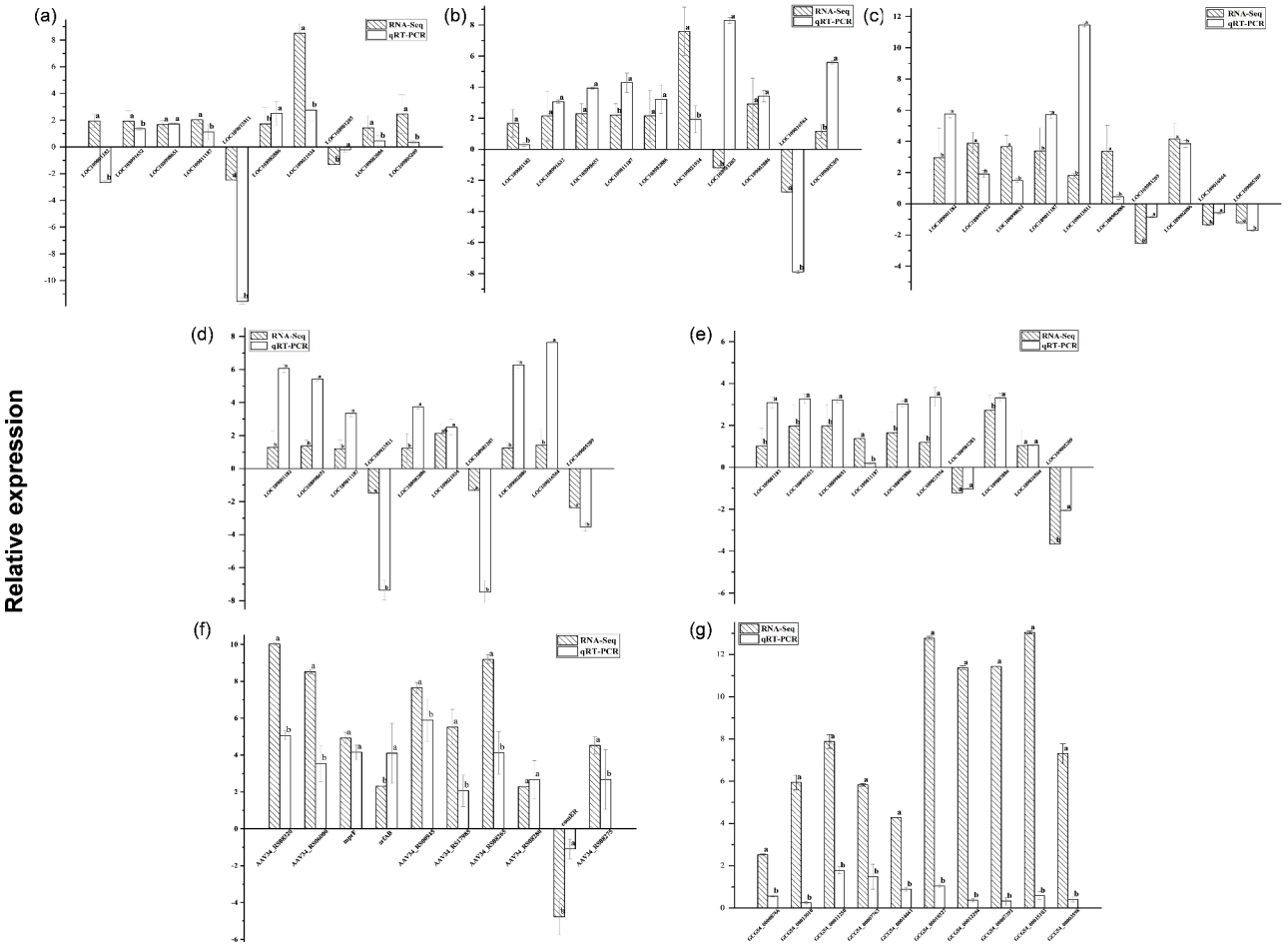

Fig. 10 Validation of transcriptome sequencing data by quantitative real-time PCR (qRT-PCR). (**a**)-(**e**). The qRT-PCR results of 10 differentially expressed genes in the comparison groups of walnut B vs. C, T vs. C, TB vs. C, TB vs. T, and TB vs. B, respectively. (**f**). The qRT-PCR results of 10 differentially expressed genes of *Bacillus velezensis*. (**g**). The qRT-PCR results of 10 differentially expressed genes of *Colletotrichum gloeosporioides*. The values represent the mean ± standard deviation of three biological replicates. Different letters indicate significant differences among different varieties at the $p < 0.05$ level

[34]. Our results reveal that *B. velezensis* treatment significantly enhances walnut resistance to *C. gloeosporioides*. Under the treatment of *B. velezensis*, the inoculation of walnuts with *C. gloeosporioides* (TB vs. B) exhibited enriched metabolic processes, including small molecule, drugs, and amino acid metabolism (Fig. 3d), and induced the expression of more disease-resistant related genes and hormones in plants in the plant-pathogen interaction and plant hormone signal transduction pathways (Figs. 3 and 4). Notably, the genes RPS2 and RPM1, known to confer broad-spectrum resistance to pathogenic fungi, bacteria, and pests in rice [35], showed significantly higher induction in TB vs. C compared to T vs. C (Fig. 4a), suggesting *B. velezensis* potentiates ETI responses of walnut. Furthermore, *B. velezensis* activated the MEKK1-MKK1/MKK2-MPK4 cascade, with MEKK1 upregulation in B vs. C, TB vs. C, and TB vs. T comparison groups and MPK6 upregulation in TB vs. T indicating PTI activation (Fig. 4b) [36, 37]. Downregulation of PYL and upregulation of ABF and EIN3 in B vs. C, TB vs. C, and TB vs. T comparison groups groups (Fig. 4b) imply coordinated regulation of ABA and ethylene signaling, consistent with their roles in stress adaptation [38–41]. These results suggest that *B. velezensis* can regulate plant hormones such as abscisic acid and ethylene in response to the invasion of *C. gloeosporioides* to enhance plant resistance.

Conclusion

This study presents a tripartite RNA-Seq analysis of the "Walnut-*C. gloeosporioides*-*B. velezensis*" system, systematically characterizing transcriptional interactions among the host, pathogen, and biocontrol agent. Through comparative analysis of four treatment conditions (untreated control, *C. gloeosporioides* inoculation, *B. velezensis* inoculation, and co-inoculation), we identified three key interaction mechanisms: (i) The pathogen hub gene CGS of *C. gloeosporioides* showed negative regulation by *B.*

velezensis concomitant with actin cytoskeleton activation and synaptic vesicle cycle suppression; (ii) *B. velezensis* upregulated hub genes srfAC and purB increasing the production and secretion of antibacterial substances under pathogen challenge; (iii) Dual inoculation synergistically activated host defense pathways, inducing pathogenesis-related genes and enhancing hormone-mediated resistance (ETI, PTI, ISR) through MAPK signaling. These findings establish the first transcriptomic framework for tripartite interactions in plant disease systems, providing molecular foundation for biocontrol strategies against walnut anthracnose.

Abbreviations

DEGs	Differentially expressed genes
WGCNA	Weighted gene coexpression network analysis
PPI	Protein-protein interaction
GO	Gene ontology
KEGG	Kyoto encyclopedia of genes and genomes
TCA cycle	Citric acid cycle
JA/ET	Jasmonic acid/ethylene
LB	Lysogeny broth
PDA	Potato dextrose agar
UMI	Unique identifier
RPKM	Reads per kilobase per million mapped reads
qRT-PCR	Quantitative real-time polymerase chain reaction
MAPK	Mitogen-activated protein kinase
ETI	Effector-triggered immunity
PTI	Pattern-triggered immunity
ISR	Induced systemic resistance

Supplementary Information

The online version contains supplementary material available at https://doi.org/10.1186/s12870-025-06565-z.

Supplementary Material 1

Acknowledgements
Not applicable.

Author contributions
S.W.W. and T.H.Z. conceived the idea and revised the manuscript. S.W.W. collected the experimental materials, drew figures and drafted the manuscript. S.Y.L. and H.M.Y.Z. helped in drawing figures and drafting the manuscript. All authors listed have made direct and substantial efforts for improving the manuscript and approved the final version.

Funding
This research was supported and funded by the Yaan Science and Technology Program (No. 23ZDYF0002) and the Natural Science Foundation of Sichuan Province (No. 2024NSFSC1193).

Data availability
The RNA sequencing data are available via NCBI with BioProject accession PRJNA1030780 and PRJNA1216589.

Declarations

Ethics approval and consent to participate
Not applicable.

Consent for publication
Not applicable.

Competing interests
The authors declare no competing interests.

Received: 3 February 2025 / Accepted: 15 April 2025
Published online: 17 May 2025

References

1. Hsieh TF, Shen YM, Huang JH, Tsai JN, Lu MT, Lin CP. Insights into grape ripe Rot: A focus on the *Colletotrichum gloeosporioides* species complex and its management strategies. Plants. 2023;12(15):2873.
2. Mehmood N, Yuan Y, Ali MM, Iftikhar AMM, Cheng J. Early transcriptional response of terpenoid metabolism to *Colletotrichum gloeosporioides* in a resistant wild strawberry *Fragaria nilgerrensis*. Phytochemistry. 2021;181:112590.
3. Sudheeran PK, Sela N, Carmeli-Weissberg M, Ovadia R, Panda S, Feygenberg O, et al. Induced defense response in red Mango fruit against *Colletotrichum gloeosporioides*. Hortic Res. 2021;8(1):17.
4. Ramos AP, Talhinhas P, Sreenivasaprasad S, Oliveira H, Ramos AP, Talhinhas P, et al. Characterization of *Colletotrichum gloeosporioides*, as the main causal agent of citrus anthracnose, and C. karstii as species preferentially associated with lemon twig dieback in Portugal. Phytoparasitica. 2016;44(4):549–61.
5. Wang QH, Fan K, Li DW, Han CM, Qu YY, Qi YK, et al. Identification, virulence and fungicide sensitivity of *Colletotrichum gloeosporioides* S.s. Responsible for walnut anthracnose disease in China. Plant Dis. 2020;104(5):1358–68.
6. Gan P, Ikeda K, Irieda H, Narusaka M, O'Connell RJ, Narusaka Y, et al. Comparative genomic and transcriptomic analyses reveal the hemibiotrophic stage shift of *Colletotrichum fungi*. New Phytol. 2013;197(4):1236–49.
7. Soriano-Hernandez AD, Madrigal-Perez DG, Galvan-Salazar HR, Arreola-Cruz A, Briseño-Gomez L, Guzmán-Esquivel J, et al. The protective effect of peanut, Walnut, and almond consumption on the development of breast Cancer. Gynecol Obstet Invest. 2015;80(2):89–92.
8. Balakireva AV, Zamyatnin AAJ. Indispensable role of proteases in plant innate immunity. Int J Mol Sci. 2018;19(2):629.
9. Choub V, Ajuna HB, Won SJ, Moon JH, Choi SI, Maung CEH, et al. Antifungal activity of *Bacillus velezensis* CE 100 against anthracnose disease (*Colletotrichum gloeosporioides*) and growth promotion of walnut (*Juglans regia* L.) trees. Int J Mol Sci. 2021;22(19):10438.
10. Li ZJ, Tang SY, Gao H, Ren JY, Xu PL, Dong WP, et al. Plant growth-promoting rhizobacterium *Bacillus cereus* AR156 induced systemic resistance against multiple pathogens by priming of camalexin synthesis. Plant Cell Environ. 2024;47(1):337–53.
11. Jumpathong W, Intra B, Euanorasetr J, Wanapaisan P, Jumpathong W, Intra B, et al. Biosurfactant-Producing *Bacillus velezensis* PW192 as an Anti-Fungal biocontrol agent against *Colletotrichum gloeosporioides* and *Colletotrichum Musae*. Microorganisms. 2022;10(5):1017.
12. Kim YS, Lee Y, Cheon W, Park J, Kwon HT, Balaraju K, et al. Characterization of *Bacillus velezensis* AK-0 as a biocontrol agent against Apple bitter rot caused by *Colletotrichum gloeosporioides*. Sci Rep. 2021;11(1):626.
13. Kang X, Guo Y, Leng S, Xiao L, Wang L, Xue Y, et al. Comparative transcriptome profiling of *Gaeumannomyces Graminis* Var. *Tritici* in wheat roots in the absence and presence of biocontrol *Bacillus velezensis CC09*. Front Microbiol. 2019;10:1474.
14. Yacoub A, Magnin N, Gerbore J, Haidar R, Bruez E, Compant S, et al. The biocontrol Root-Oomycete, *Pythium Oligandrum*, triggers grapevine resistance and shifts in the transcriptome of the trunk pathogenic fungus, *Phaeomoniella Chlamydospora*. Int J Mol Sci. 2020;21(18):6876.
15. Mortazavi A, Williams BA, McCue K, Schaeffer L, Wold B, Mortazavi A, et al. Mapping and quantifying mammalian transcriptomes by RNA-Seq. Nat Methods. 2008;5(7):621–8.
16. Langfelder P, Horvath S. WGCNA: an R package for weighted correlation network analysis. BMC Bioinformatics. 2008;9(1):559.
17. Shannon P, Markiel A, Ozier O, Baliga NS, Wang JT, Ramage D, et al. Cytoscape: a software environment for integrated models of biomolecular interaction networks - PubMed. Genome Res. 2003;13(11):2498–504.
18. Gai Y, Li L, Ma H, Riely BK, Liu B, Li H. Critical role of MetR/MetB/MetC/MetX in cysteine and methionine metabolism, fungal development, and virulence of *Alternaria alternata*. Appl Environ Microbiol. 2020;87(4):e01911–20.
19. Liu LG, Ding ZJ, Li MH, Wu CH, Xie XJ, Peng J, et al. Functional analysis of cystathionine gamma-synthase in *Fusarium oxysporum* F. Sp. *cubense*. Mycosystema. 2023;42(7):1575–87.

20. Berepiki A, Lichius A, Read ND. Actin organization and dynamics in filamentous fungi. Nat Rev Microbiol. 2011;9(12):876–87.
21. Zhang Y, An B, Wang W, Zhang B, He C, Luo H, et al. Actin-bundling protein fimbrin regulates pathogenicity via organizing F-actin dynamics during appressorium development in *Colletotrichum gloeosporioides*. Mol Plant Pathol. 2022;23(10):1472–86.
22. Liu N, Wang W, He C, Luo H, An B, Wang Q. NADPH oxidases play a role in pathogenicity via the regulation of F-Actin organization in *Colletotrichum gloeosporioides*. Front Cell Infect Microbiol. 2022;12:845133.
23. Jung H, Gkogkas Christos G, Sonenberg N, Holt Christine E. Remote control of gene function by local translation. Cell. 2014;157(1):26–40.
24. Rishal I, Fainzilber M. Axon–soma communication in neuronal injury. Nat Rev Neurosci. 2013;15(1):32–42.
25. Saito A, Cavalli V. Signaling over distances. Mol Cell Proteom. 2016;15(2):382–93.
26. Lin Y, Briandet R, Kovács ÁT. *Bacillus cereus* sensu Lato biofilm formation and its ecological importance. Biofilm. 2022;4:100070.
27. Ishvaria S, Dharshini RS, Manickam R, Pooja KR, Ramya M, Ishvaria S, et al. Draft genome sequencing and functional annotation and characterization of biofilm-producing bacterium *Bacillus novalis* PD1 isolated from rhizospheric soil. Antonie Van Leeuwenhoek. 2021;114(12):1977–89.
28. Che JM, Lai GT, Xu H, He LY, Li SY, Chen BX, et al. Identification of the chorismic acid synthetase gene *BbaroC* in *Brevibacillus brevis* and analysis of the transcription factor regulation. Fujian Agricultural Sci Technol. 2024;55(1):8–17.
29. Chi BK, Huyen NTT, Loi VV, Gruhlke MCH, Schaffer M, Mäder U, et al. The disulfide stress response and protein S-thioallylation caused by allicin and Diallyl polysulfanes in *Bacillus subtilis* as revealed by transcriptomics and proteomics. Antioxidants. 2019;8(12):605.
30. Yang H, Wang H, Wang F, Zhang K, Qu J, Guan J, et al. Efficient extracellular production of Recombinant proteins in *E. coli* via enhancing expression of *DacA* on the genome. J Ind Microbiol Biotechnol. 2022;49(4):kuac016.
31. Scholz R, Vater J, Budiharjo A, Wang Z, He Y, Dietel K et al. Amylocyclicin, a novel circular bacteriocin produced by Bacillus amyloliquefaciens FZB42. J Bacteriol. 2014-3-7;196(10).
32. Rungsirivanich P, Parlindungan E, O'Connor PM, Field D, Mahony J, Thongwai N et al. Simultaneous Production of Multiple Antimicrobial Compounds by *Bacillus velezensis* ML122-2 Isolated From Assam Tea Leaf [*Camellia sinensis* var. *assamica* (J.W.Mast.) Kitam.]. Frontiers in Microbiology. 2021/11/24;12.
33. Dimopoulou A, Theologidis I, Benaki D, Koukounia M, Zervakou A, Tzima A, et al. Direct antibiotic activity of bacillibactin broadens the biocontrol range of *Bacillus amyloliquefaciens* MBI600. mSphere. 2021;6(4):00376–21.
34. Rabbee MF, Ali MS, Choi J, Hwang BS, Jeong SC, Baek K-h, et al. *Bacillus velezensis*: A valuable member of bioactive molecules within plant microbiomes. Molecules. 2019;24(6):1064.
35. Li Z, Huang J, Wang Z, Meng F, Zhang S, Wu X, et al. Overexpression of *Arabidopsis* Nucleotide-Binding and Leucine-Rich repeat genes *RPS2* and *RPM1*(*D505V*) confers Broad-Spectrum disease resistance in rice. Front Plant Sci. 2019;10:00417.
36. Sun L, Zhang J. Regulatory role of receptor-like cytoplasmic kinases in early immune signaling events in plants. FEMS Microbiol Rev. 2020;44(6):845–56.
37. Bi G, Zhou Z, Wang W, Li L, Rao S, Wu Y, et al. Receptor-Like cytoplasmic kinases directly link diverse pattern recognition receptors to the activation of Mitogen-Activated protein kinase cascades in Arabidopsis. Plant Cell. 2018;30(7):1543–61.
38. Wang YH, Que F, Li T, Zhang RR, Khadr A, Xu ZS, et al. DcABF3, an ABF transcription factor from Carrot, alters stomatal density and reduces ABA sensitivity in Transgenic *Arabidopsis*. Plant Sci. 2021;302:110699.
39. Rao S, Tian Y, Xia X, Li Y, Chen J. Chromosome doubling mediates superior drought tolerance in *Lycium ruthenicum* via abscisic acid signaling. Hortic Res. 2020;7(1):40.
40. Zhu Z, An F, Feng Y, Li P, Xue L et al. A M,. Derepression of ethylene-stabilized transcription factors (EIN3/EIL1) mediates jasmonate and ethylene signaling synergy in *Arabidopsis*. Proceedings of the National Academy of Sciences. 2011;108(30):12539-44.
41. Aluko OO, Ninkuu V, Ziemah J, Jianpei Y, Taiwo E, Ninkuu SB, et al. Genome-wide identification and expression analysis of EIN3/EIL gene family in rice (*Oryza sativa*). Plant Stress. 2024;12:100437.

Publisher's note